Geo-information Science and Remote Sensing

Thesis Report GIRS-2024-24

Assessing Forest Recovery Following Selective Logging-related Tropical Forest Disturbances using Sentinel-1 Radar Data

Siti Syarafina Yuliandari

Frontpage image: Retrieved September 7th 2023, from
https://www.recoveryways.com/rehab-blog/the-healing-forest-our-recovery-community/

26 March 2024

Assessing Forest Recovery Following Selective Logging-related Tropical Forest Disturbances using Sentinel-1 Radar Data

Siti Syarafina Yuliandari

1242202

Supervisors:

dr. Johannes Reiche

Johannes Balling, MSc.

A thesis submitted in partial fulfillment of the degree of Master of Science
at Wageningen University and Research,
The Netherlands.

March 26 2024
Wageningen, The Netherlands

Thesis code number: GRS-80436
Thesis Report: GIRS-2024-24
Wageningen University and Research
Laboratory of Geo-Information Science and Remote Sensing

Acknowledgements

Alhamdulillah. *This has been a pleasant journey in the past 7 months.* Firstly, I would like to express my gratitude to Johannes Reiche and Johannes Balling (Mecki) for their guidance and inspiration throughout this research journey. Working alongside them has been truly enjoyable, as it felt like a collaborative effort rather than working under someone. One of the main reasons I chose Wageningen University was my experience using RADD Alerts in previous work, which left me amazed by its domain. From that moment on, I had a goal to collaborate with Johannes in the radar data domain, and I'm delighted to have achieved that goal with the completion of this research.

To my biggest supporters, my dear Mama, Papa, and Vira, I want to express my heartfelt gratitude for your support and prayers. Even though we haven't seen each other in almost two years, I have always felt close to you because of your prayers. Your encouragement has been the reason I've persevered until now. I hope that I can make you proud.
To Syifa, my dearest best friend, I want to express my heartfelt gratitude for your unwavering presence by my side throughout all the ups and downs. Let's continue this journey together. And to Fikria, Noura, and Nia, thank you for being such wonderful friends who have always supported and trusted me, whether during our holidays or our time together here.

Lastly, I would like to express my heartfelt gratitude to the Wageningen University Fellowship Programme and the Anne van den Ban Scholarship Fund for selecting and trusting me as one of their scholarship recipients. It is thanks to their support that my dream of studying for a master's degree here has become a reality.

Abstract

Selective logging has emerged as the second leading cause of forest disturbance in West Papua, Indonesia. Understanding forest recovery is essential in order to support land management planning and conservation efforts. Studies investigating large-scale forest recoveries commonly rely on optical sensors, while the potential of radar data remains understudied. Contrary to optical data, the radar signal is capable of penetrating parts of the tree foliage, allowing for an improved assessment of the status of the vegetation structure.

In this study, we investigate the signal recovery of Sentinel-1 (C-band radar) data for selective logging-related forest disturbances in West Papua, Indonesia. Forest disturbances were based on the RADD alerts and further manually classified into four classes (road horizontal, road vertical, large-sized, and small-sized logging events). A method was developed to assess the signal recovery of backscatter for each disturbance type, initially focusing on temporal recovery and incorporating spatial analysis. Furthermore, the recovery process was characterized using three commonly employed recovery metrics for optical data.

We presented a method capable of assessing the signal recovery of Sentinel-1. Road verticals exhibit a longer recovery time than road horizontals, which is attributed to radar shadow effects. Conversely, small logging events demonstrate faster recovery times than large ones. The findings show that the edge of the logged area recovers faster than the interior, whether it is a logging road or logging events. Lastly, the study demonstrates that three spectral recovery metrics, originally applied in optical imagery, can effectively be used in radar data, providing diverse insights into signal recovery.

Contents

Acknowledgements

Abstract i

List of Figures v

List of Tables v

Acronyms and Abbreviation vi

1 Introduction 1
- 1.1 Context and Background . . . 1
- 1.2 Literature Review . . . 1
  - 1.2.1 Signal Recovery . . . 1
  - 1.2.2 Recovery Metrics . . . 2
  - 1.2.3 Sentinel-1 Radar for Forest Disturbance and Regrowth . . . 2
- 1.3 Research Objectives . . . 3

2 Study Area 4

3 Data 5
- 3.1 Sentinel-1 . . . 5
- 3.2 RADD Alerts . . . 5
- 3.3 PlanetScope Data . . . 5

4 Methodology 6
- 4.1 Preparing Data . . . 6
  - 4.1.1 Defining Types of Logging-related Forest Disturbances . . . 6
  - 4.1.2 Specifying Period of Time Series . . . 7
  - 4.1.3 Preprocessing Data . . . 9
- 4.2 Detecting and Mapping Signal Recovery . . . 9
- 4.3 Characterizing Signal Recovery . . . 10
  - 4.3.1 Analysing Side-looking Geometry and Spatial Orientation on Signal Recovery . . . 10
  - 4.3.2 Temporal Features of Signal Recovery . . . 10
  - 4.3.3 Comparison of Different Recovery Metrics . . . 11

5 Results 12
- 5.1 Signal Recovery Status . . . 12
- 5.2 Exploring Factors Influencing Signal Recovery . . . 13
  - 5.2.1 The Effect of Side-Looking Radar and Spatial Orientation . . . 15
- 5.3 Analysis of Recovery Levels . . . 20
- 5.4 Comparison of Different Recovery Metrics . . . 22

6 Discussions **24**
6.1 RQ1: Signal Recovery Detected and Its Duration 24
6.2 RQ2: Influencing Factors on Signal Recovery 24
6.3 RQ3: Signal Recovery Characterization 25
6.4 SAR for Monitoring Forest Recovery 26

7 Limitations and Recommendations **28**

References **32**

List of Figures

1 Study area of four sub-districts in West Papua with a zoom-in showing selective logging and logging roads in close proximity (blue box). 4
2 Overview of the Methodology 6
3 Types of Disturbances 7
4 Pre-disturbance, disturbance period, and post-disturbance period based on a Sentinel-1 backscatter time series. The green boxes show the signal recovered zone (which is explained in 4.2) 8
5 Points lie within the recovery zone (blue color) classified as recovered, while red shows no recovery. 10
6 Three recovery metrics 11
7 Signal Recovery measured for both polarizations and orbits. The red line is the mean, and the blue line is the median. 12
8 The Signal Recovery Mapping (showing the results of Descending VH). 13
9 Signal Recovery for various disturbance types for both polarizations and orbits 14
10 Geometric Effects on Selective logging-related disturbances. The illustration radar shadow (bottom) is taken from Bouvet et al. (2018). The image was obtained on May 5th, 2020, with a range from -20 dB to 0 dB. . . 15
11 Illustration on VV and VH polarization. Road Horizontal on Sentinel-1 backscatter images, with a range from -20 dB to 0 dB for VV and a range from -30db to -5 db for VH polarization. Illustration of double bounce and volume scattering, is taken from Zhao et al. (2016). 19
12 Signal Recovery Mapping in an example area: Red Indicates Not-recovered Pixel, Green Indicates Recovered Pixel. 20
13 A map of spatial patterns of signal recovery representing percentage recovered. 21
14 Spatial and Temporal Recovery for Disturbance Types (Site a and Site b) 21
15 Recovery Metrics for Various Disturbances (Descending VV). Median value shown in a (+) marker. 22
16 Mean Value of Three Recovery Metrics for Various Disturbances (Descending VV). 22
17 Comparison Three Recovery Metrics for all types in Descending VV . . 23

List of Tables

1 Recovery Metrics 11
2 Percentage of Pixel Recovered 12
3 Number of Pixels 14
4 Radar Scattering in Road Horizontal 16
5 Radar Scattering in Road Vertical 17
6 Radar Scattering in Large-sized Logging Events 18
7 Radar Scattering in Small-sized Logging Events 18

Acronyms and Abbreviation

ANOVA Analysis of Variance

FRI2 Forest Recovery Index 2

GEE Google Earth Engine

LiDAR Light Detection and Ranging

NBR Normalized Burn Ratio

NDMI Normalized Difference Moisture Index

NDVI Normalized Difference Vegetation Index

SAR Synthetic-Aperture Radar

TCG Tasselled Cap Greenness

R80p Ratio of Eighty Percent

RADD Radar for Detecting Deforestation

RRI Relative Recovery Index

YrYr Year on Year Average

Y2R Years to Recovery

VV Year on Year Average

1 Introduction

1.1 Context and Background

Forest disturbances in Indonesia are predominantly attributed to several processes, including but not limited to fire occurrences, peatland drainage, deforestation activities, and the creation of plantations dedicated to palm oil or timber production (Romijn et al., 2013). These activities contribute to both local and global land cover change, exacerbating the loss of primary forest cover, which, in turn, accelerates biodiversity loss and carbon emissions (Aguilar-Amuchastegui et al., 2014). According to data from GlobalForestWatch (2023), West Papua experienced loss of 55.7 thousand hectares of humid primary forest between 2018 and 2022. The Teluk Bintuni district is ranked second in terms of tree cover loss in the province of West Papua, Indonesia.

Logging activities play a crucial role in the loss of the remaining forest in the region of Papua and Kalimantan (Turubanova et al., 2018). In Papua, from 2001 to 2018, selective logging emerged as the second most prominent factor contributing to forest disturbances. This was primarily caused by timber extraction activities, involving the selective removal of economically valuable trees and resulting in the formation of small canopy gaps near logging roads. In addition, approximately 12% of the overall reduction in forest areas has been deforested nearby (within a 1-kilometer radius) to major roadways since 2000 (Gaveau, 2018).

Monitoring selective-logging related disturbances can provide significant insights for land-use planning and the development of conservation initiatives. As one of the components of many conservation efforts, recovery of forests can contribute to the sequestration of atmospheric carbon, mitigation of carbon emissions, and augmentation of ecosystem resilience in climate-related disasters (Raharjo et al., 2022).

Remote sensing has proven to be a valuable tool for detecting forest disturbances and monitoring post-disturbance forest recoveries at large scale (Zhao et al., 2016). Optical and radar remote sensing sensors are capable of capturing different aspects of forest recovery due to their different sensitivities towards forest structure (radar) or photosynthetic activity (optical) (Frolking et al., 2009; Surovỳ and Kuželka, 2019).

1.2 Literature Review

1.2.1 Signal Recovery

Forest recovery refers to the process wherein a forest ecosystem regains its structure, composition, and ecological functionalities following a disturbance event, such as fire, logging activities, or natural disasters (Flores et al., 2017). While forest recovery and signal recovery are connected, understanding their linkages across different sensing methods is still lacking. Many remote sensing studies have investigated the post-forest disturbance signal recovery, but only 5% of these studies utilized radar data compared to 80% using optical data (Kurbanov et al., 2022). Often, the signal recovery for optical or radar data only represents a partial aspect of the recovery process, such as re-greening in optical data or the structural regrowth of smaller vegetation in radar data. For

instance, Jones and Schmitz (2009) found that full recovery for forest ecosystems take approximately 42 years.
Researchers evaluate forest recovery by studying changes in remote sensing signals over time. One example of this is the study conducted by Chirici et al. (2020), who utilized remote sensing data to evaluate the rate of spectral signal recovery in clear-cut areas inside Mediterranean coppice forests. By concentrating on signal recovery, we can analyze immediate and intermediate changes through remote sensing data. This approach provides detailed insights into the initial stages and subsequent progression of recovery after logging activities.

1.2.2 Recovery Metrics

Several studies have explored metrics to characterize and measure signal recovery (Pickell et al., 2016; Meng et al., 2018; Morresi et al., 2019; De Keersmaecker et al., 2022; White et al., 2022). Pickell et al. (2016) used the R80p (Ratio of Eighty Percent) metric on Landsat time-series data and spectral indices, such as NDVI and NBR, to evaluate forest recovery. Various recovery metrics were also assessed to see a comparison of recovery metrics on assessing forest recovery, for instance, FRI2 (Forest Recovery Index 2) with Pearson correlation coefficient by Morresi et al. (2019) and De Keersmaecker et al. (2022) who used three recovery metrics, such as: YrYr (Year on Year Average), R80p (Ratio of Eighty Percent) and RRI (Relative Recovery Index). These recovery metrics are useful for characterizing the process of forest recovery. For instance, Chirici et al. (2020) found that the Y2R metric based on both NBR and NDVI showed similar characterizations of rapid recovery in the studied coppice-managed areas of forest management.

Nevertheless, only a few studies utilized radar signals to evaluate forest recovery, and none of them have applied the recovery metrics mentioned earlier. Radar signals have the capability to effectively penetrate cloud cover, thereby enabling the acquisition of data even under almost all weather conditions. An interesting instance is provided by Tanase et al. (2011), who conducted a study on post-fire forest regrowth utilizing SAR and employed Analysis of Variance (ANOVA) as a statistical tool to evaluate the forest recovery based on mean values of SAR backscatter and coherence.

1.2.3 Sentinel-1 Radar for Forest Disturbance and Regrowth

Many studies have employed radar remote sensing, specifically Sentinel-1, to detect forest disturbance in tropical forests (Antropov et al., 2016; Reiche et al., 2021; Aquino et al., 2022; Doblas et al., 2022). Here, Sentinel-1 data has demonstrated its potential for operational monitoring of fine-scale disturbances in near-real time. For instance, RADD (Radar for Detecting Deforestation) Alerts was developed (Reiche et al., 2021). Contrary to forest disturbance detection and characterization based on Sentinel-1 data, the recovery of fine-scale disturbance (e.g., selective logging) using Sentinel-1 remains largely understudied. Moreover, the Sentinel-1 satellite employs side-looking radar, meaning it observes forest disturbance and recovery differently based on the orientation of linear events. Side-looking radar leads to radiometric and geometric effects. Geometric

effects include phenomena like radar shadow and foreshortening, which are caused by the angle of incidence of the radar signal relative to the terrain and objects on the ground (Bamler, 2000). Shadows, characterized by a sudden drop in backscatter within the Sentinel-1 time series, are useful for detecting disturbances (Bouvet et al., 2018). For instance, a study conducted by Bouvet et al. (2018) demonstrated the utilization of radar shadow analysis, based on patch orientation, to detect deforestation. Furthermore, observations are also influenced by surface scattering, which involves the interaction of radar waves with surface features (Park et al., 2014). The interaction between radar shadow and surface scattering can affect appearance of radar shadows and effect on detect recovery. This study aims to assess forest recovery and analyze the impact of radar shadow and foreshortening on this process while also adapting established recovery metrics from optical remote sensing to the context of Sentinel-1 backscatter data.

1.3 Research Objectives

This research aims to understand the signal recovery, particularly fine-scale selective logging-related disturbances, including logging roads and logging events detected by the RADD Alert system in four districts in Teluk Bintuni, West Papua, Indonesia. Through the analysis of dense Sentinel-1 backscatter time series data, the study seeks to characterize the temporal patterns and spatial extent of signal recovery in the study areas.

Research Questions

1. Does the backscatter signal recover to a similar pre-disturbance level, and what is the recovery duration?

2. How do the side-looking radar geometry and spatial orientation of disturbance events (e.g., roads) affect signal recovery?

3. Can recovery metrics be used to characterize the spatial and temporal patterns of signal recovery?

This research defines 'signal recovery' as the state where the remote sensing signal reaches the pre-disturbance signal level. The first research question is addressed using a temporal moving window approach to assess whether the backscatter values at the pixel level have recovered to their pre-disturbance level and estimate the recovery's duration. Then, this study examined the impact of side-looking radar and spatial orientation on signal recovery in selective logging. Lastly, the characteristics of recovery metrics will be analyzed for different types of disturbances.

2 Study Area

The study area of this research is located in four different districts (Biscoop, Dataran Beimes, Manimeri, Merdey) in Teluk Bintuni regency, West Papua Province, Indonesia (Figure 1). In West Papua, selective logging activities from 2001 to 2018 led to the loss of 56,700 hectares (Gaveau, 2018) and were one of the major factors in the decline of mangrove forest disturbance in Teluk Bintuni (Yudha et al., 2021). The study area spans 411.642 hectares, located between 1.830°S - 1.347°S latitude and 132.952°E - 133.650°E longitude. The methodology was developed in the Merdey district and further tested in the three additional districts.

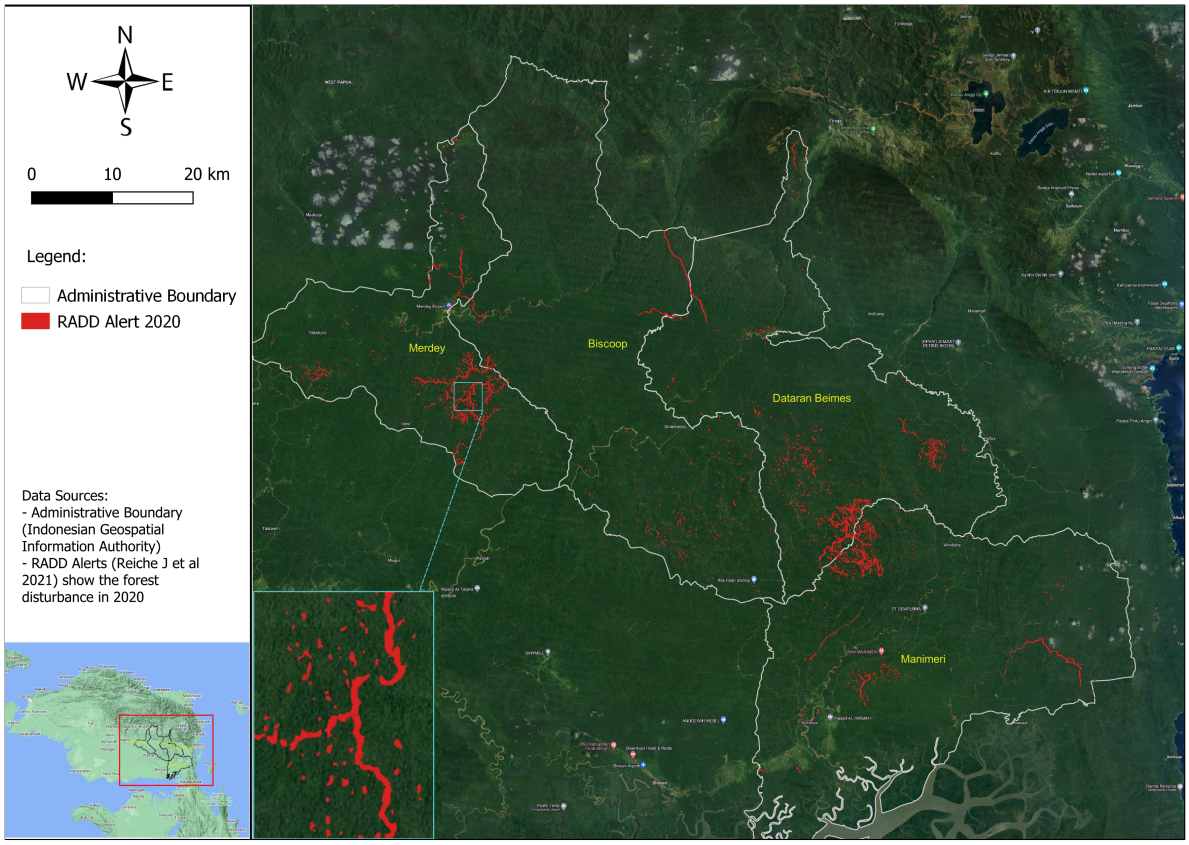

Figure 1: Study area of four sub-districts in West Papua with a zoom-in showing selective logging and logging roads in close proximity (blue box).

3 Data

3.1 Sentinel-1

Sentinel-1A/B is a constellation of two-polar orbiting satellites that operate day and night, utilizing C-band synthetic aperture radar (SAR) (Filipponi, 2019). However, as of the end of 2022, only Sentinel-1A remains operational. Sentinel-1 acquires ascending orbits, which travel from south to north, and descending orbits, which travel from north to south. The assessment focused on data acquired in Interferometric Wide swath mode. The C-band SAR equipment on Sentinel-1 provides imagery with a pixel spacing of 10 meters and a spatial resolution of approximately 20 x 22 m. Additionally, the temporal resolution of Sentinel-1 data, referring to the revisit time, typically ranges from 6 to 12 days in the tropics and can be even faster in Europe. This research utilizes data with dual polarization (VV+VH) (ESA, 2022).
Sentinel-1 satellite images are the primary data in this research, using Level-1 Ground Range Data (GRD). All available images from January 2017 to February 2024 were used. With only Sentinel-1A operating, the temporal resolution was up to 12 days in the tropics.

3.2 RADD Alerts

RADD alerts, a near real-time alerting system based on Sentinel-1 data, deliver forest disturbance alerts updated with each new Sentinel-1 observation. This research used the RADD alerts from Reiche et al. (2021) to detect instances of forest disturbances across both geographical locations and time periods. Alerts are confirmed within a maximum 90-day period if the probability of forest disturbance is above 97.5%, indicating high confidence. The current geographic coverage of RADD alerts includes humid tropical forests in several countries across South America, Central America, Africa, Southeast Asia, and the Pacific.

3.3 PlanetScope Data

In October 2017, Planet successfully launched three distinct satellite constellations, offering very high-resolution (VHR) multispectral data with a resolution of 3.7 meters and high temporal resolution, enabling frequent revisits to the same area for near real-time monitoring and analysis (PlanetTeam, 2017). The PlanetScope imagery from these constellations was integrated into the research process to manually distinguish logging road disturbances.

4 Methodology

Figure 2 shows an overview of the methodology of this research. This research initially defined types of selective logging-related forest disturbance using high-resolution Planet imagery. Then, followed by processing Sentinel-1 time series data. Subsequently, this study developed a pixel-based method to detect signal recovery using a temporal moving window approach to address RQ1. Then, it involved the analysis of side-looking radar data and the spatial orientation to understand the differences in signal recovery for various disturbance types, addressing RQ 2. Lastly we assessed the potential characterization of recovery via several recovery metrics, typically applied in optical imagery, can be utilized in radar imagery.

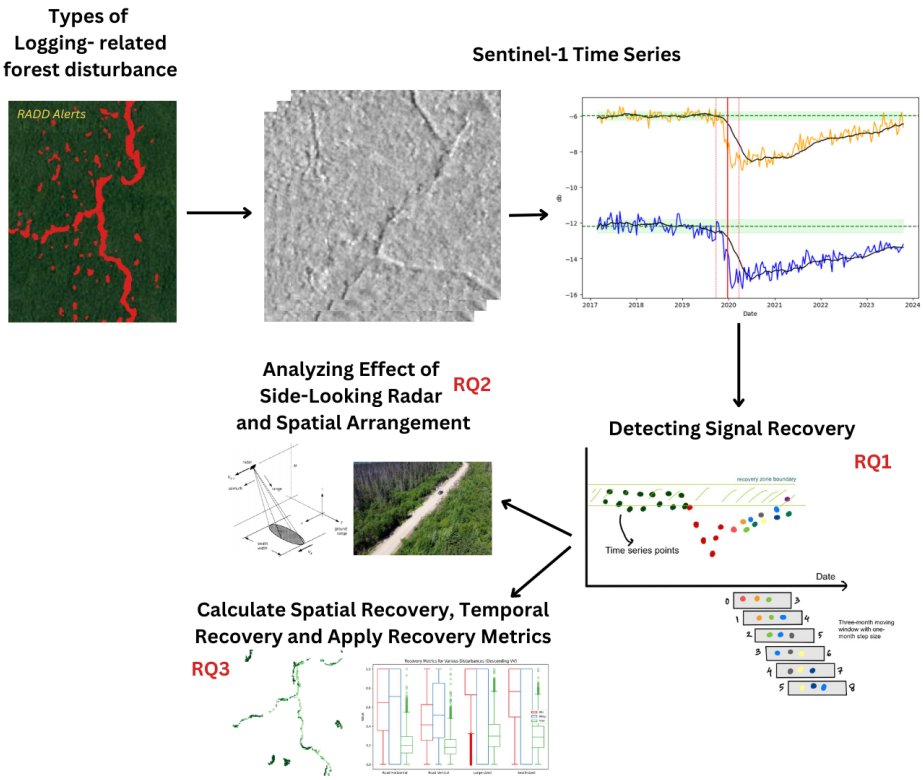

Figure 2: Overview of the Methodology

4.1 Preparing Data

4.1.1 Defining Types of Logging-related Forest Disturbances

Selective logging-related disturbances include logging roads and smaller disturbance patches of canopy gaps along logging roads (logging events). In order to assess how the side-looking radar geometry affects the recovery signal of differently oriented disturbance events (parallel or perpendicular to the line of sight of the radar sensor), forest disturbance events were categorized into, such as road horizontal, road vertical, large-sized events, and small-sized events. Separating vertical and horizontal roads is a simplification, as the sensor does not fly perfectly from north to south but instead has an inclination of approximately 11 degrees (Schaufler et al., 2018). Therefore, the look direction is

not precisely 90 degrees. The division of large and small-sized events to examine the differences in signal recovery on different sizes of logging events. The methodology for dividing logging roads and logging events involved the following steps:

1. Manually digitizing horizontal and vertical oriented road segments by examining high-resolution images (PlanetScope).

2. Calculating the area of RADD alerts in spatial proximity to logging roads. Events with an area ranging from 0.1 to 0.5 hectares were classified as small-size events, while those greater than 0.5 hectares were classified as large-sized events.

Subsequently, backscatter values for each pixel were extracted based on the RADD alert polygons for each disturbance, to be used in the next processes. The division of these disturbances can be further explored in the table below.

Image	**Type**	**Description**
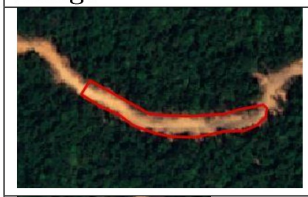	Road Horizontal	Logging roads are characterized by a predominantly about 90-degree angle (horizontal). These roads typically traverse the terrain in a left-to-right or right-to-left direction.
	Road Vertical	Logging roads are characterized by a predominantly 0-degree angle (vertical). These roads typically traverse the terrain in an up-and-down, down-and-up, or oblique direction.
	Large-sized logging events	Disturbances that encompass an area greater than 0.5 hectares.
	Small-sized logging events	Disturbances that encompass an area between 0.1 and 0.5 hectares

Figure 3: Types of Disturbances

4.1.2 Specifying Period of Time Series

This research assesses the recovery of RADD forest disturbance events that occurred in 2020 and analyzes the backscatter data for every pixel from January 2017 to February 2024. The period from 2017 - 2019 was used as a historical baseline, and the period

following the disturbance was used to study the signal recovery. Figure 4 provides an illustration of three periods of time series (pre-disturbance period, disturbance period, and post-disturbance period). Due to the lengthy processing time, this study simplified the RADD information (as it was in day-of-year format) to a monthly format. For example, a polygon with RADD format dates ranging from 20001 to 20031 would have the 31st of January 2020 assigned as its disturbance date, while a polygon from 20032 to 20061 would have the 29th of February 2020 assigned as its **disturbance date**, and so forth.

The period from 2017 up to six months before the disturbance date is referred to as the **pre-disturbance period** (refer to Figure 4). This decision was made to ensure that the pre-disturbance phase accurately represents undisturbed conditions. Including the time period immediately preceding the disturbance detection might introduce noise or confounding factors related to the disturbance event itself, as well as potential delays in detection caused by remaining post-disturbance debris or tree remnants (Balling et al., 2023). This period is used as the baseline for non-disturbed pixels.

This study defines the **post-disturbance period** as six months after the detected disturbance until February 2024 (the end of the monitoring period). This consideration is crucial because moisture fluctuations may result in high backscatter values after the detected disturbance date (Harfenmeister et al., 2019), potentially influencing the interpretation of the 'recovered signal'. The **disturbance period** refers to the time when the disturbance began and includes fluctuations that occur after the disturbance. Therefore, each RADD alert dataset polygon is associated with distinct disturbance date, pre-disturbance, and post-disturbance period. Figure 4 provides an illustrative example of these periods for one pixel.

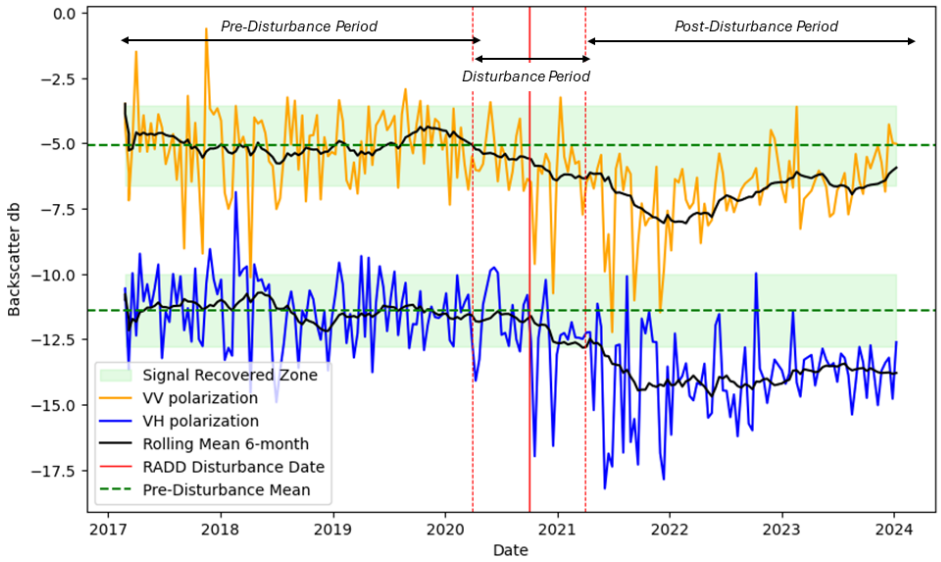

Figure 4: Pre-disturbance, disturbance period, and post-disturbance period based on a Sentinel-1 backscatter time series. The green boxes show the signal recovered zone (which is explained in 4.2)

4.1.3 Preprocessing Data

Before ingesting Sentinel-1 data into Google Earth Engine (GEE), preprocessing steps were already conducted to derive the backscatter coefficient in decibels (dB) using the Sentinel-1 Toolbox. Additional pre-processing steps were applied to generate the analysis-ready data (ARD) concept, including border noise correction, lee-speckle filtering, and radiometric terrain normalization (Mullissa et al., 2021).

Planet data was accessed via the Education and Research Program via GEE. Planet data's preprocessing includes automatic atmospheric correction and cloud masking (PlanetTeam, 2017). A six-month rolling mean was employed to reflect the recovery process to reduce the effect of environmental influences, such as moisture fluctuations. The resulting smoothed data is then utilized in subsequent processes involving a moving window.

4.2 Detecting and Mapping Signal Recovery

The primary objective of research question 1 is to assess whether pixels have recovered to their pre-disturbance levels and then to determine the duration required for this recovery. We adopt the approach of Tanase et al. (2011) and only used mean values for each moving window.

The concept of a moving window is akin to the rolling mean used in data preprocessing and is also applied in assessing signal recovery. It involves selecting a subset of data points within a designated window that moves through the dataset over time. Statistical measures like mean and standard deviation are calculated for each window, allowing for data analysis of trends, patterns, and temporal variations. A three-month moving window with a one-month step size is used in this process.

We calculated the mean and standard deviation of the pre-disturbance period. Then, the recovery zone was established for each pixel by computing the upper and lower boundaries as the mean $\pm$ the standard deviation, respectively (refer to Figure 4). Signal recovery was reached when five consecutive mean data points and their standard deviations within the recovery zone. The pixel is classified as recovered if both the first and last five consecutive points are within the recovery zone. This approach accounts for the possibility of fluctuations in signal intensity, ensuring that the recovery classification is based on a sustained improvement. The choice of five consecutive data points deviates from the approach used by Decuyper et al. (2022), who employed three consecutive dates to denote 'regrowth.' The decision to use five consecutive data points was made to ensure a more conservative and robust assessment of signal recovery. A longer duration of consecutive data points allows for a more thorough evaluation of the stability of the recovered signal.

Signal recovery detection was conducted on a pixel basis, resulting in thousands of pixels for each type of disturbance, with recovered or non-recovered. Here is an example of points lying within the recovery zone.

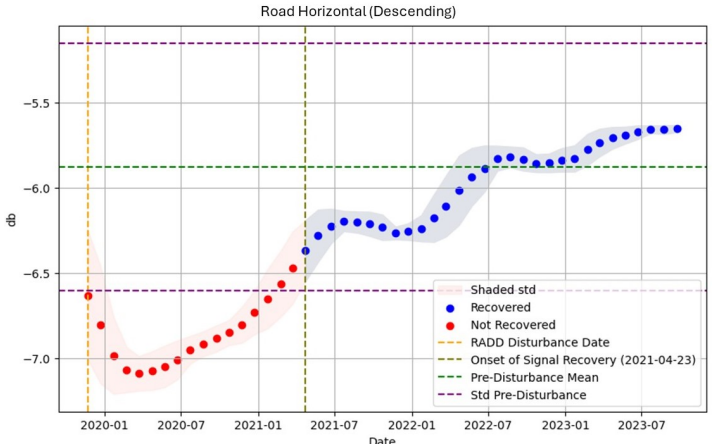

Figure 5: Points lie within the recovery zone (blue color) classified as recovered, while red shows no recovery.

The signal recovery mapping aims to illustrate the temporal variability and extent of recovery per pixel in response to various types of disturbances. We assess the maximum percentage recovered for each pixel, the duration for each pixel to reach full recovery, and a comparison of recovery metrics across pixels.

4.3 Characterizing Signal Recovery

Characterizing signal recovery entails understanding its attributes across various time period and factors affecting it, and comparing or correlating with three spectral recovery metrics.

4.3.1 Analysing Side-looking Geometry and Spatial Orientation on Signal Recovery

After determining whether the signal has recovered or not, the next step involves analyzing factors that affect signal recovery for different disturbances. Two key factors under consideration are **side-looking radar** and **spatial orientation**. Side-looking radar refers to polarization, orbit and geometry effects such as shadowing and foreshortening. Furthermore, spatial orientation includes factors such as the layout of logging roads (including skid roads) and the orientation of logging events and logging roads. Skid road is a temporary road constructed for timber extraction during selective logging operations (Sidle et al., 2004). These two factors are not separate from each other but are interrelated in how they influence the recovery of signals for different types of disturbances.

4.3.2 Temporal Features of Signal Recovery

After employing a moving window approach to assess the recovery status of each pixel (explained in 4.2), this study also calculated the percentage recovery and temporal recovery to illustrate which period that each pixel of disturbance types reached full recovery. The study identified patterns or differences in the signal recovery process by comparing recovery across different types of disturbances.

4.3.3 Comparison of Different Recovery Metrics

This research adopts a similar approach from Frazier et al. (2018) and De Keersmaecker et al. (2022), which applied three spectral recovery metrics (R80p, RRI and YrYr) metrics using NBR values and Landsat time series in Canadian boreal forest and Amazon tropical forest respectively.

The resulting values for these metrics are normalized to the range from 0 to 1. For RRI, a value of zero indicates no signal recovery, while a value of one indicates equal amounts of recovery and disturbance. Similarly, R80p values range from zero, indicating no recovery, to one, indicating backscatter values have recovered to 80% of their pre-disturbance levels. Lastly, the YrYr metric reflects the average annual change after disturbance. A YrYr value of zero signifies no signal recovery over the three-year period, while positive values indicate average backscatter gain over three years. The equation (which was modified by Frazier et al. (2018)) and description of each metric can be seen in the figure and table below.

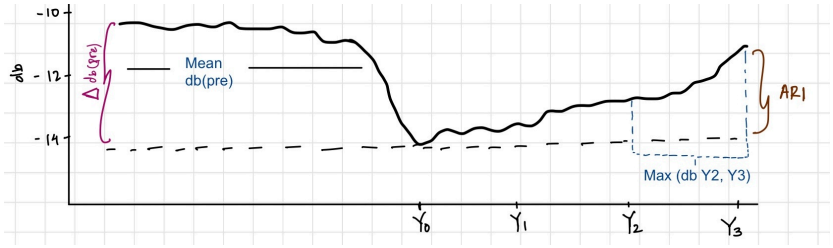

Figure 6: Three recovery metrics

Table 1: Recovery Metrics

Metric	Equation	Description
R80p	$R80p = \frac{Max(dbY2, Y3)}{0.8 * Meandb(pre)}$	The maximum backscatter value (Max(db Y2, Y3)) is determined by obtaining the maximum value during the post-disturbance period, which occurs in either the second or third year after the disturbance. Furthermore, compared to the 80% pre-disturbance average of the backscatter values.
RRI	$RRI = \frac{ARI}{\Delta db(pre)}$	ARI (Absolute Recovery Index) is calculated as the maximum backscatter value in the post-disturbance period reduced by the backscatter value in the disturbance period. Then, divided by the magnitude of change in the pre-disturbance period.
YrYr	$YrYr = \frac{db(Y3) - db(Y0)}{3}$	Backscatter value in the third year after disturbance substracted by backscatter value in the year of disturbance (Y0). Then, divided by the number of years.

5 Results

This subsequent outlines the findings of this study. In Section 5.1, the study addressed whether the signal had recovered or not and its duration. Section 5.2 provided insights into the characterization of signal recovery, considering factors such as geometry effects and types of disturbances. Lastly, 5.3 and 5.4 delved into explaining the signal recovery level and comparing three recovery metrics.

5.1 Signal Recovery Status

As described in 4.2, a method was developed to classify each pixel in selective logging-related disturbances as 'recovered' or 'not recovered'. The table below shows the proportion of pixels recovered without considering the type of disturbance period.

Table 2: Percentage of Pixel Recovered

Category	**Proportion of Pixel Recovered**
Descending VV	87.3%
Descending VH	78.9%
Ascending VV	76.3%
Ascending VH	64.4%

Furthermore, refer to 4.3.2, this study has mapped temporal variability to characterize signal recovery and ascertain the duration required for full signal recovery, as seen in the figure below.

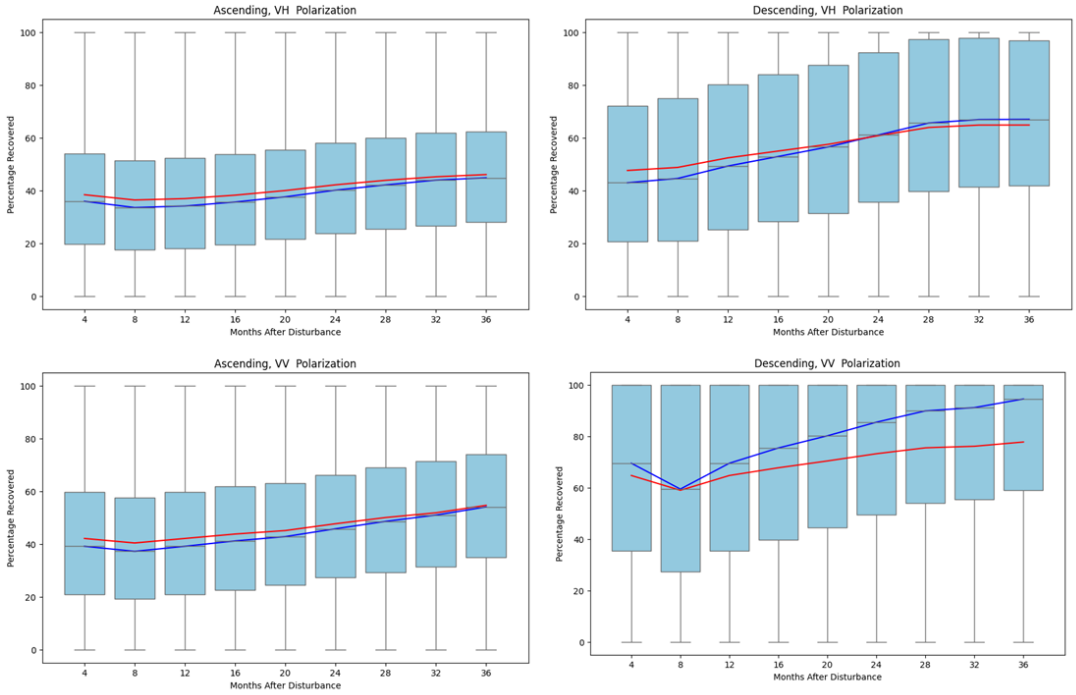

Figure 7: Signal Recovery measured for both polarizations and orbits. The red line is the mean, and the blue line is the median.

Boxplots offer a concise summary of central tendency, spread, and outlier presence, making them useful for comparing distributions across multiple groups. The box in boxplot represents the interquartile range (IQR), with the lower and upper edges indicating the 25th and 75th percentiles, respectively. In Descending VV polarization, the upper 25% of data fully recovered within four months, while in Descending VH, the upper data full recovery occurred after two years. However, in both Ascending polarizations, the majority of pixels only reached a maximum of around 60% recovery.

The red and blue line chart depicting the mean and median signal recovery percentage respectively, provides a more straightforward visualization of the overall trend in signal recovery. The median of Descending VV pixels indicates 94% recovery in the last month of post-disturbance period (36 months after disturbance), and the average trend across both orbits and polarizations show a maximum signal recovery of only 66%. The figure below illustrates 92% signal recovery for descending VH in relation to selective logging-related disturbances over a three-year period from January 2020 to February 2024.

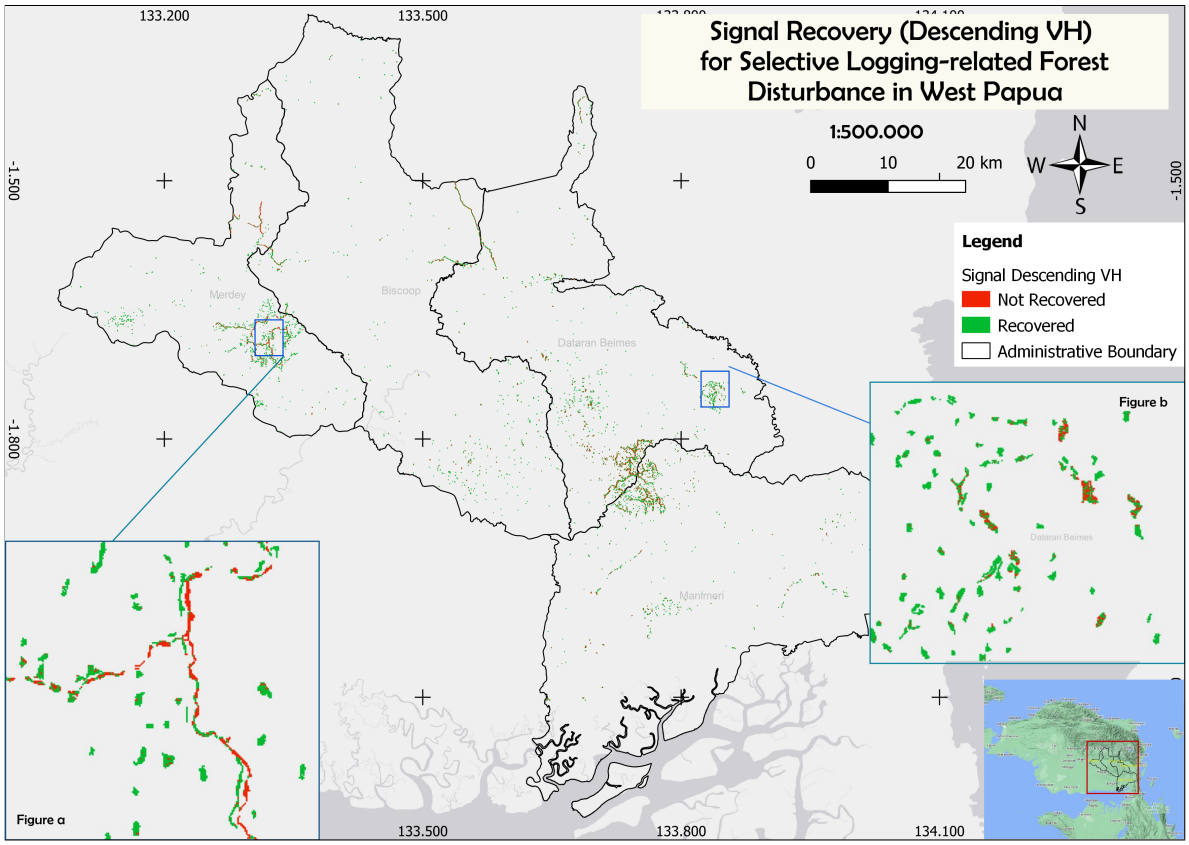

Figure 8: The Signal Recovery Mapping (showing the results of Descending VH).

5.2 Exploring Factors Influencing Signal Recovery

As explained in Section 4.2, the detecting signal recovery was pixel-based for each type of disturbance. The accumulation of total pixels for the development area (Merdey district) and the testing areas (Biscoop, Dataran Beimes, and Manimeri districts) is

presented in the table below.

Table 3: Number of Pixels

Type	**Total Pixels**	**Proportion of Total Pixels**
Road Horizontal	8468	8.7%
Road Vertical	25173	26%
Large-sized logging events	24286	25.1%
Small-sized logging events	38968	40.2%

Small-sized logging events accounted for 40% of the coverage area, with 38968 pixels calculated. The assessment of the upper 25% data has full recovery for descending VV or 60% signal recovery for ascending orbits. As shown in Figure 7, the proportion of small-size logging events is the reason why we observe the top quartile of the data has complete signal recovery in descending VV. The image below illustrates the signal recovery for various types of disturbances.

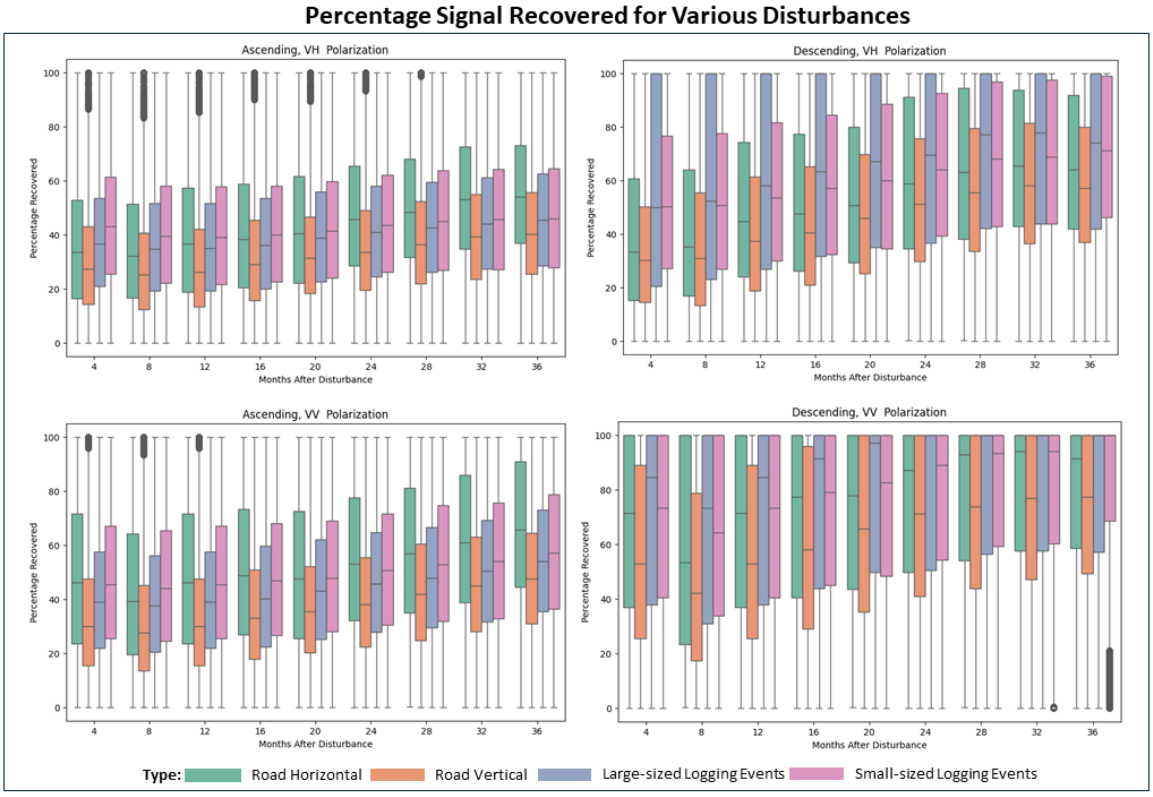

Figure 9: Signal Recovery for various disturbance types for both polarizations and orbits

As observed in Figure 9, the majority of pixels for all types have not fully recovered in the Ascending orbit for both polarizations. In the Descending VV orbit, the upper 25% of data for all types have fully recovered after two years, except for road vertical. Conversely, in Descending VH, only the upper 25% of data for large-sized events have fully recovered.

5.2.1 The Effect of Side-Looking Radar and Spatial Orientation

The differences in signal recovery across different orbits and polarizations are seen in the previous section and are explained in this section. This study assesses why there is a difference in signal recovery based on how the spatial orientation observed by the side-looking radar (geometric effects, polarization, and orbit) affects signal recovery.

Geometric Effects in Ascending and Descending

This section elucidates how geometric effects in descending and ascending orbits contribute to the observed differences in signal recovery. The image below shows the geometric effects, such as foreshortening and shadowing. **Foreshortening** can cause features to appear compressed or shortened along the radar line of sight. In this case, the white pixels appear as a slope in the area of the vertical road, which suggests that foreshortening may be distorting the appearance of the road.

The area where the radar signal cannot reach is depicted as a **Radar Shadow**. The black pixel, indicated by the dark blue arrow, represents the shadow where the surrounding forest obstructs the logging events. The figure about how shadow appears in ascending and descending orbit, modified from the original image from Bouvet et al. (2018). As the satellite travels from south to north with a right-looking antenna in an Ascending orbit, the borders between forest and non-forest regions, observed from west to east, appear as shadow areas. Conversely, in a Descending orbit, as the satellite travels from north to south, with borders between forest and non-forest regions observed from east to west, they are perceived as shadow areas (Bouvet et al., 2018).

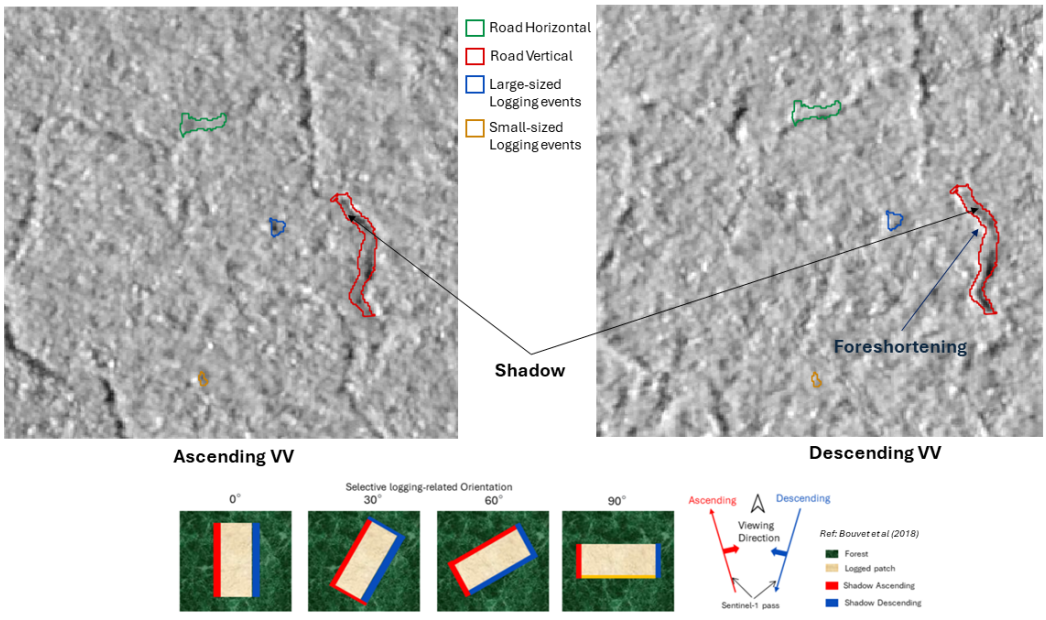

Figure 10: Geometric Effects on Selective logging-related disturbances. The illustration radar shadow (bottom) is taken from Bouvet et al. (2018). The image was obtained on May 5th, 2020, with a range from -20 dB to 0 dB.

Detailed information on radar shadows for different types of disturbances can be found in Tables 4 to 7. The illustration focuses on VV polarization to demonstrate the differences in signal recovery between ascending and descending orbits.

Table 4: Radar Scattering in Road Horizontal

Sketch	PlanetScope	Ascending-VV	Descending-VV
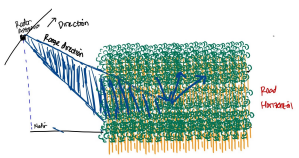		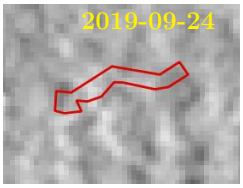	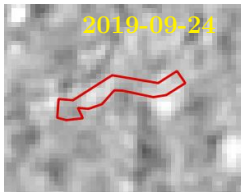
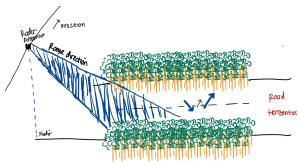		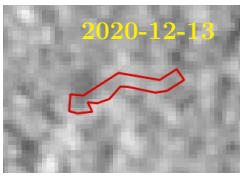	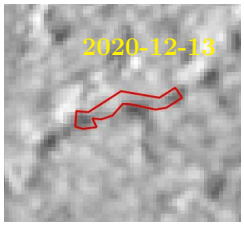
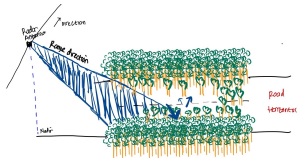		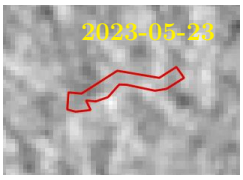	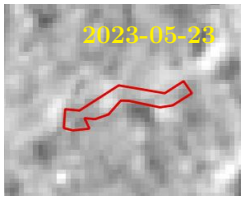

When observing a road horizontally with a side-looking radar, any disturbances along the road will likely result in a strong signal return because of surface scattering, as the radar is not obstructed by surrounding forest cover. That is because the orientation of the logging road is almost perpendicular to the side-looking radar. It is shown in high backscatter in Ascending and Descending VV on the disturbance period (2020-12-13).

Table 5: Radar Scattering in Road Vertical

Sketch	PlanetScope	Ascending-VV	Descending-VV
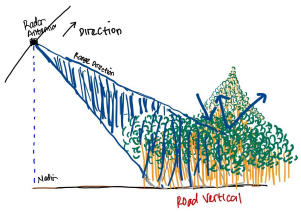		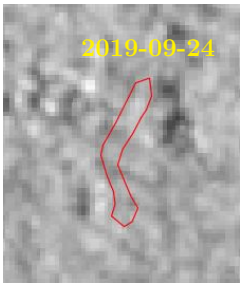	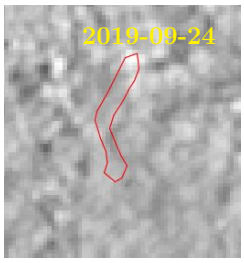
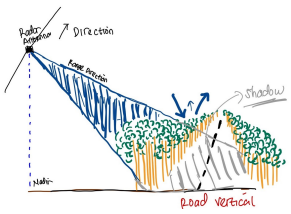		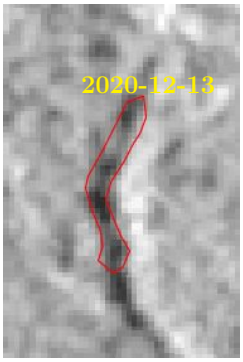	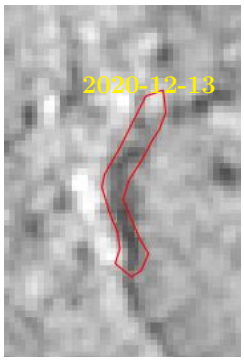
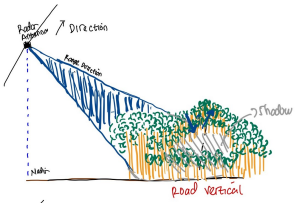		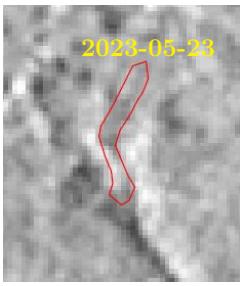	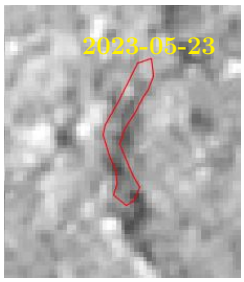

During the pre-disturbance period, there is no distinct difference in the effect of observing the road vertically with radar. The backscatter remains stable before the disturbance occurs. However, when the side-looking radar observes the road vertically during the disturbance period, there is a notable decrease in backscatter values due to radar shadowing caused by surrounding forest obstruction (refer to sketch). In the post-disturbance period (refer to the third sketch), radar shadow remains as the new growing vegetation is 'hidden' or remains obscured by the trees, resulting in a continued low backscatter value. That is why in Figure 9, the vertical road took longer to recover compared to the horizontal road.

Table 6: Radar Scattering in Large-sized Logging Events

Sketch	PlanetScope	Ascending-VV	Descending-VV
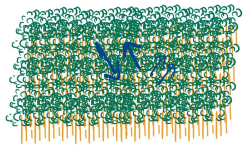		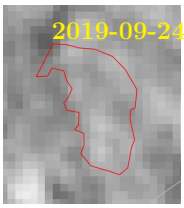	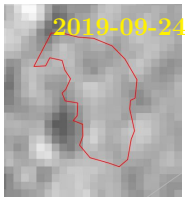
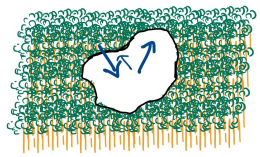	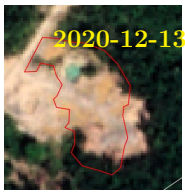	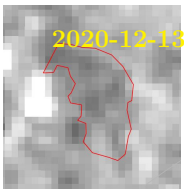	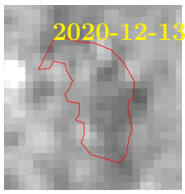
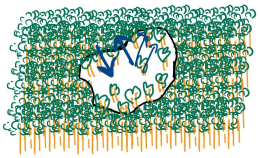		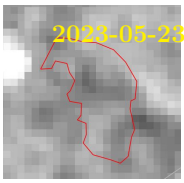	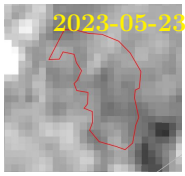

Table 7: Radar Scattering in Small-sized Logging Events

Sketch	PlanetScope	Ascending-VV	Descending-VV
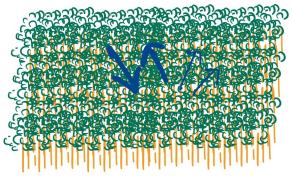		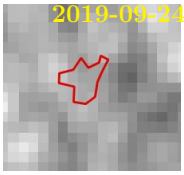	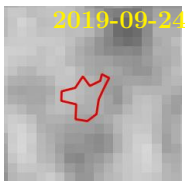
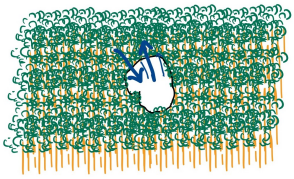		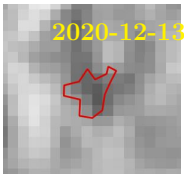	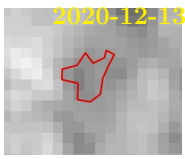
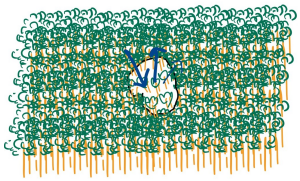		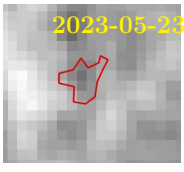	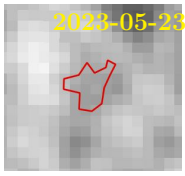

It is evident that during the pre-disturbance period, the backscatter values remained stable or exhibited similarity. However, during the disturbance period, the backscatter values in Ascending VV and Descending VV displayed heterogeneity among neighboring pixels, indicating forest disturbance. In the post-disturbance period, while some pixels still exhibit high backscatter values, others have returned to levels similar to those

observed before the disturbance for large-sized and small-sized logging events.

Effect on Polarizations

In Figure 9, it is observed that VV polarization recovers faster than VH polarization, regardless of whether it's in Ascending or Descending orbit. This is attributed to VV polarization's sensitivity to double-bounce scattering, whereas VH polarization is more sensitive to volume scattering.

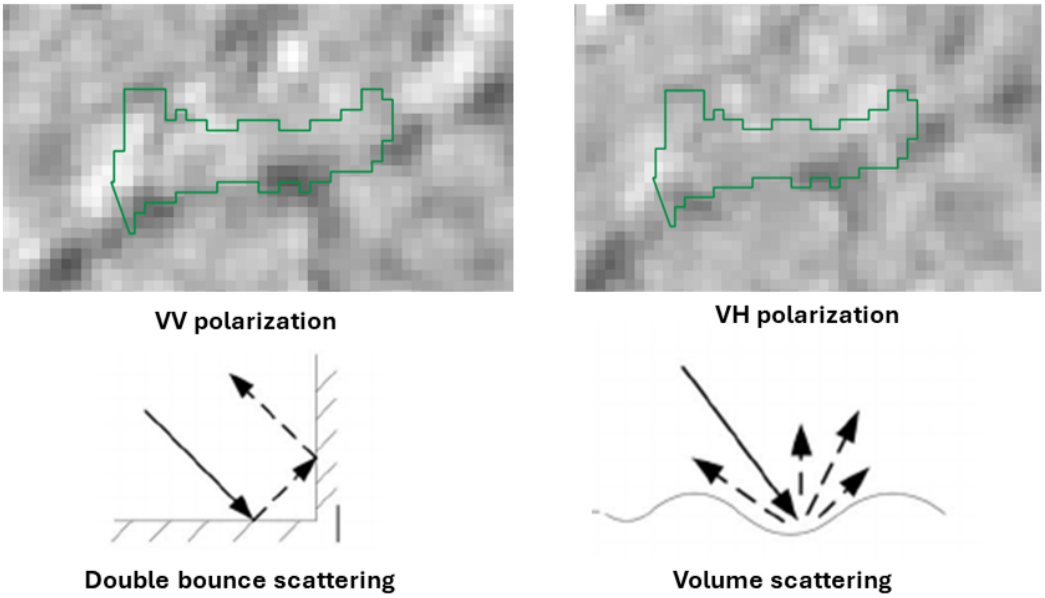

Figure 11: Illustration on VV and VH polarization. Road Horizontal on Sentinel-1 backscatter images, with a range from -20 dB to 0 dB for VV and a range from -30db to -5 db for VH polarization. Illustration of double bounce and volume scattering, is taken from Zhao et al. (2016).

The figure above shows that in VV polarization, areas exhibiting mostly surface scattering and partly double bounce scattering, which show increased backscatter intensity, resulting in brighter regions in the image. Conversely, in VH polarization, the focus shifts towards volume scattering, especially evident in areas with cut trees, stumps, and debris on the ground after logging.

Signal Recovery: Skid-roads and Logging Events Orientation

The spatial orientation is also addressed along edge lanes and skid roads. Figure 12 illustrates that road edges recover more quickly in several areas than in the interior, as shown in a purple box-shaped. This observation aligns with the discussion in the previous section, where recovery in the interior is 'hidden' due to radar shadow. Additionally, refer to Figure 9, it is shown in the figure that road horizontal (orange box-shaped) recovery is faster than road vertical (purple box-shaped) recovery.

Furthermore, as in the previous section, different orientations of logging roads were

clearly shown. It turns out that there are also different orientations of logging events. Figure 12 illustrates large-sized patches (represented by the black line) and small-sized patches (represented by the blue line). The orientation of logging events, which varies in shape, such as circular and diagonal (leaning towards vertical), influences the recovery process. For instance, in the case of large-sized number 1, more pixels remain unrecovered compared to number 2 due to its vertical shape. This difference further highlights how the perspective of the side-looking radar affects the recovery patterns.

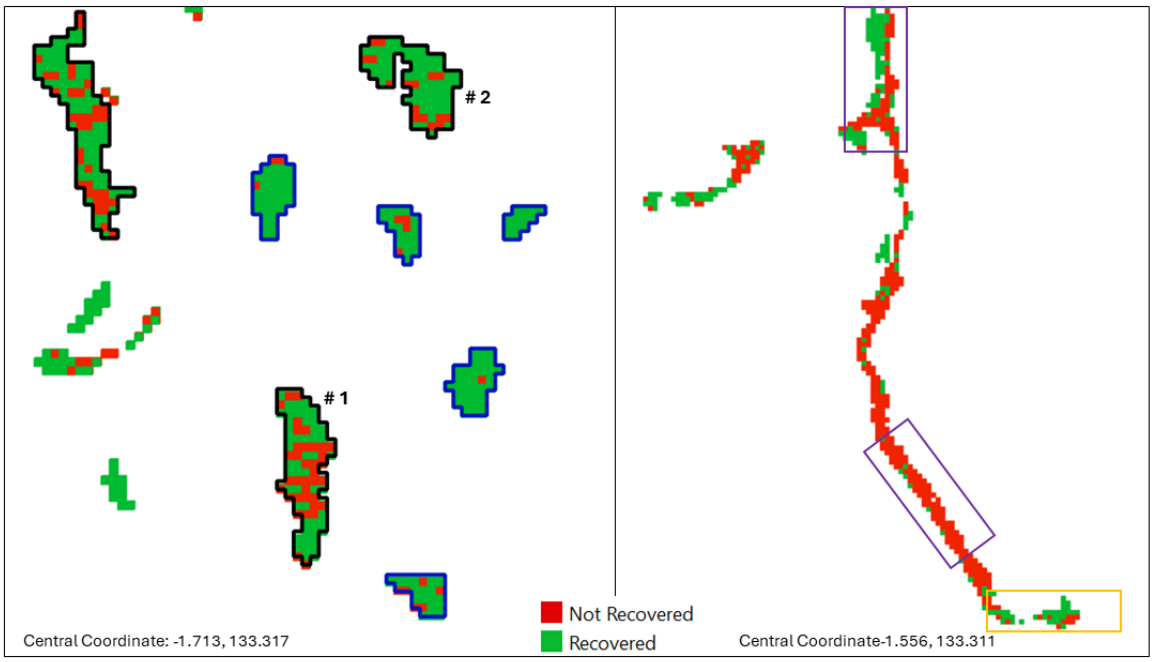

Figure 12: Signal Recovery Mapping in an example area: Red Indicates Not-recovered Pixel, Green Indicates Recovered Pixel.

5.3 Analysis of Recovery Levels

The recovery levels consist of spatial patterns of signal recovery, representing the percentage recovered for each pixel, and temporal patterns of signal recovery, indicating each pixel's recovery duration. Figure 13 depicts spatial patterns of signal recovery, illustrating the percentage of recovery for the entire study area, with a zoom-in detail focusing closely on Site A and Site B, showing the percentage recovered for different disturbance types. Site A displays the recovery for road horizontal and road vertical road disturbances. Site B illustrates recovery following large-sized and small-sized logging events.

Figure 14 shows a logging event patch (pointed by the arrow) illustrated the recovery patterns, with logging events starting at the edge and being recovered within one year, followed by the surrounding area, and the middle being recovered after two years.

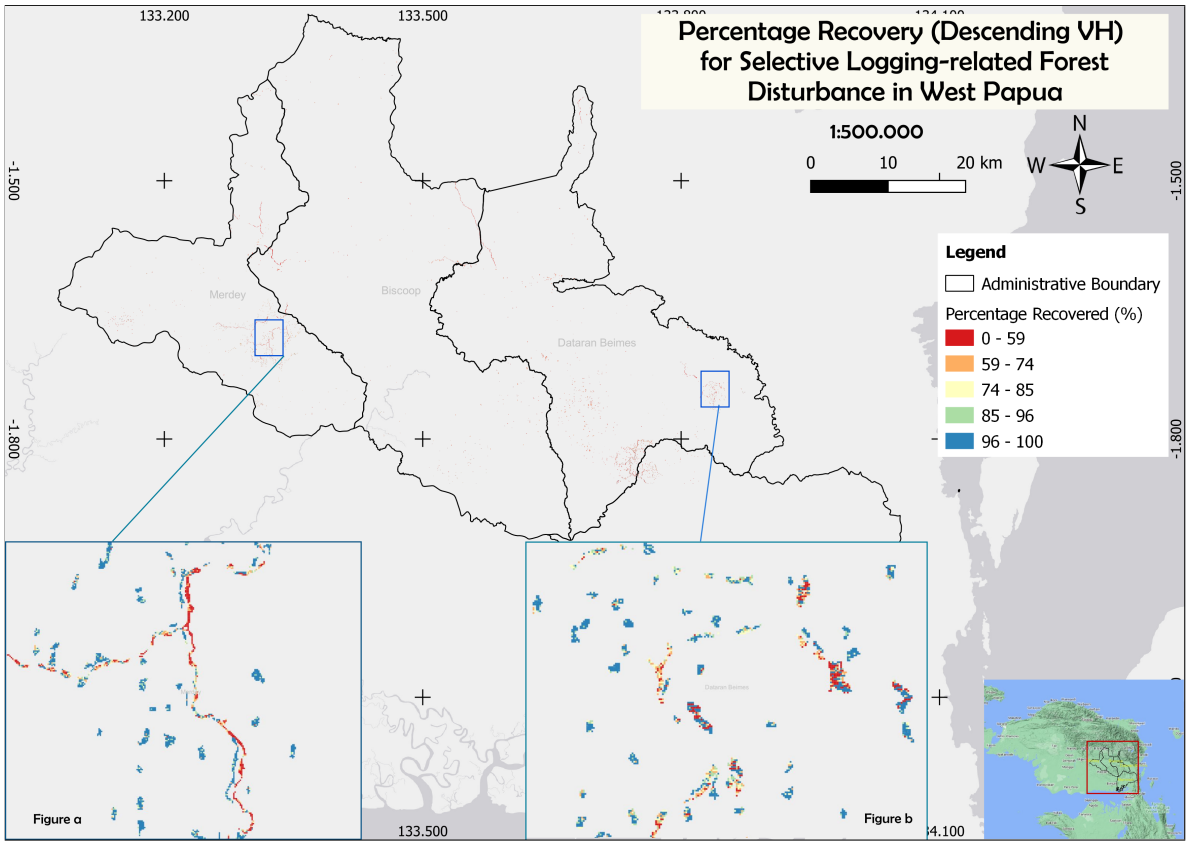

Figure 13: A map of spatial patterns of signal recovery representing percentage recovered.

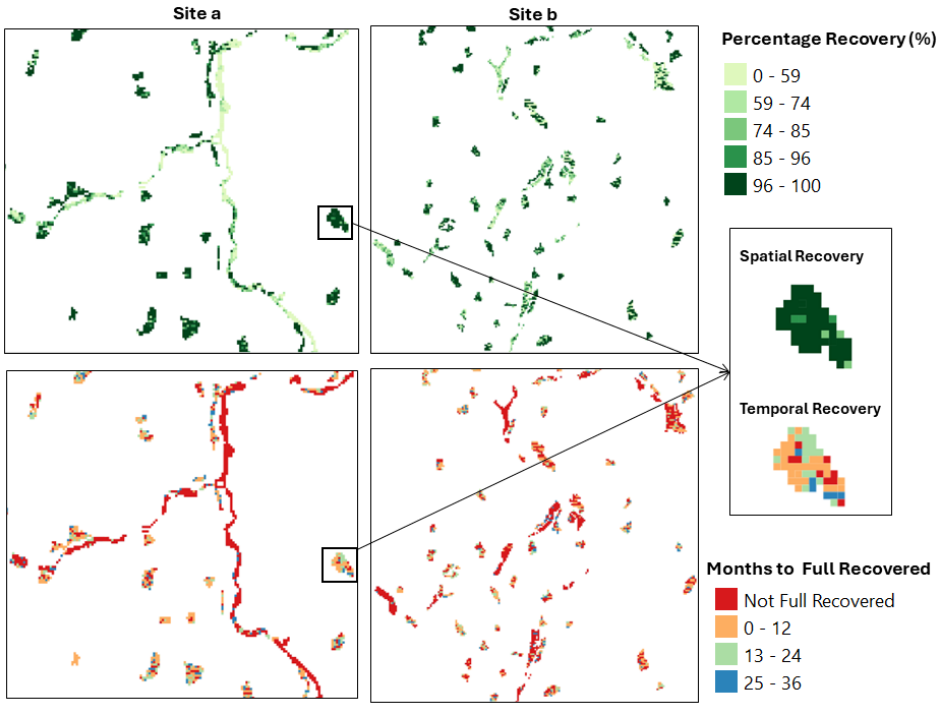

Figure 14: Spatial and Temporal Recovery for Disturbance Types (Site a and Site b)

5.4 Comparison of Different Recovery Metrics

The three metrics are calculated using the equations described in 4.3.3. The figure below is the calculation of three metrics for all types in Descending orbit and VV polarization.

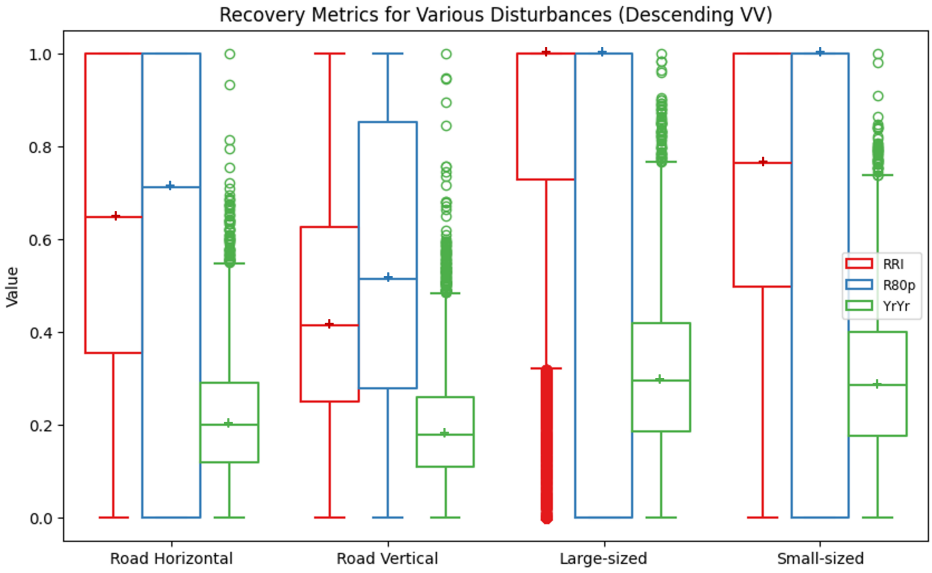

Figure 15: Recovery Metrics for Various Disturbances (Descending VV). Median value shown in a (+) marker.

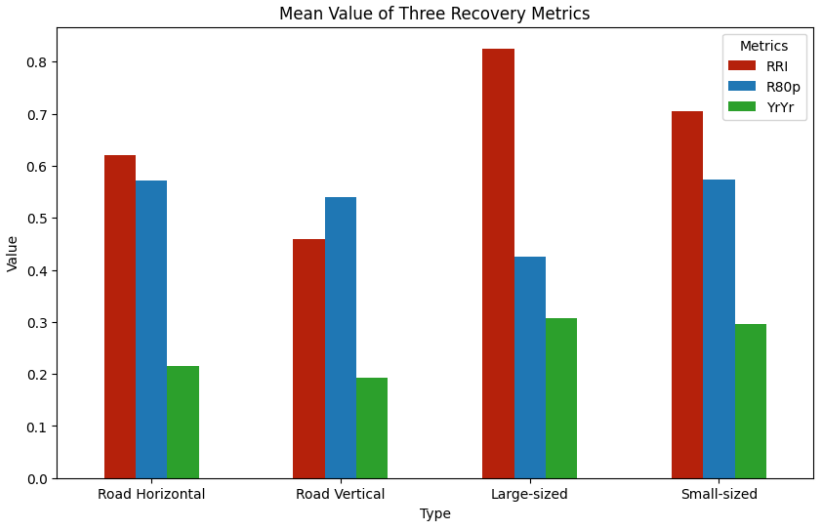

Figure 16: Mean Value of Three Recovery Metrics for Various Disturbances (Descending VV).

Figure 15 and Figure 16 display the results of three recovery metrics calculated during the last months of the post-disturbance period (Year 3). In relation to the developed method, the R80p metric exhibits similarity, with a value of 1 indicating that a pixel has

recovered to 80% of its pre-disturbance level. Referring to Figure 9, particularly in the Descending VV, the results show a similar trend, with only road vertical pixels showing a lower median and mean, while the upper quartile data of other disturbance types have recovered at least 70%. Examining the RRI metric, which assesses the magnitude of recovery in the last post-disturbance period relative to the pre-disturbance period, reveals that the upper quartile data for all disturbance types, except road vertical, show equal levels of signal recovery and disturbance occurrence. Lastly, as indicated by Frazier et al. (2018), YrYr values are typically lower than other metrics. It seems that for all disturbance types, there is a similar distribution value, indicating that average backscatter has indeed increased over the three years.

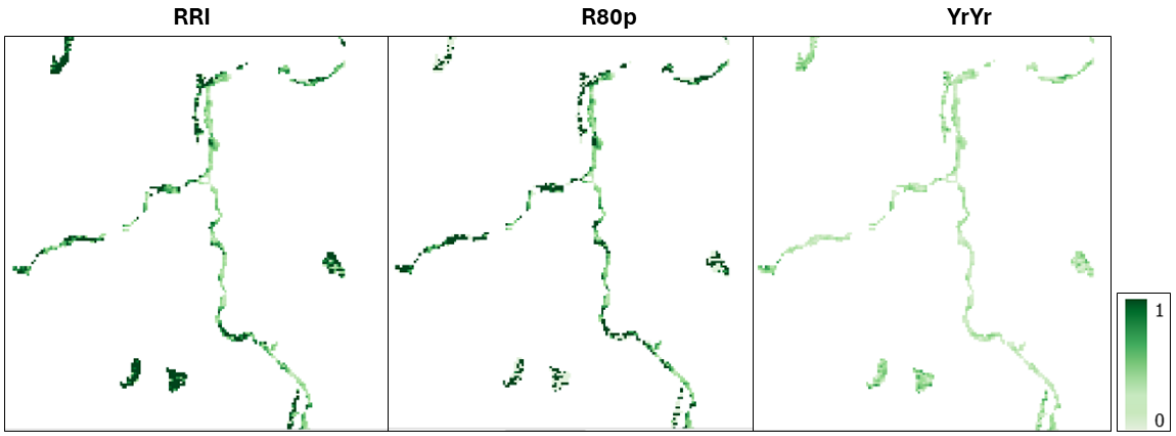

Figure 17: Comparison Three Recovery Metrics for all types in Descending VV

Figure 17 displays three recovery metrics calculated for the same area, indicating that the majority of pixels of the road have not yet fully recovered compared to the road horizontal in terms of RRI and R80p. However, for YrYr, it shows that backscatter has increased for all disturbance types over the course of three years.

6 Discussions

This section elaborates on the obtained results and how they have been integrated into the existing literature research. The first subsection addresses RQ1, focusing on the duration of signal recovery without distinguishing types of disturbance. The second subsection deals with RQ2, which involves characterizing signal recovery related to side-looking geometry radar. The final subsection compares the recovery metrics to each other (RQ3).

6.1 RQ1: Signal Recovery Detected and Its Duration

The analysis reveals that at least the top 25% data of the backscatter signal has indeed recovered to a level similar to that of the pre-disturbance period for selective logging-related disturbances (see 5.1). The proportion of recovered pixels varies across different orbits and polarizations. For instance, the ascending VH polarization shows the lowest pixel recovery rate, while the descending VV polarization reaches nearly 88% recovered. It is important to note that not all pixels have fully recovered. This research does not focus on the recovery of every individual pixel but examines the percentage of pixels that have recovered, emphasizing the majority of the data. Similarly, the duration for signal recovery varies depending on the polarization and orbit. Specifically, in the upper 25% of data in the Descending orbit, signals fully recovered within four months for VV polarization and two years for VH polarization. Conversely, in the Ascending orbit, the majority of data indicates a 60% signal recovery for either VV or VH polarization. These findings suggest that only the median value of Descending VV polarization reached 94% recovery, while other combinations of orbit and polarization reached a maximum of 66% recovery.

The developed method for detecting signal recovery utilizes a temporal moving window approach, classifying a pixel as recovered if five consecutive points lie in the post-disturbance period, a methodology similar to that described by Decuyper et al. (2022). This method establishes the pre-disturbance period as a baseline for undisturbed/stable backscatter values, akin to the approach used by R80p, as demonstrated by (Pickell et al., 2016; Frazier et al., 2018; Hird et al., 2021; De Keersmaecker et al., 2022) in assessing forest recovery. However, unlike R80p, which relies on a fixed threshold (80% of the pre-disturbance period) to classify recovery, this developed method uses the pre-disturbance period's mean and standard deviation to establish the recovery zone's boundary. This approach is similar to the method described by Frazier et al. (2015), which utilized mean and standard deviation values to categorize recovery into five categories.

6.2 RQ2: Influencing Factors on Signal Recovery

This study investigates the variation in signal recovery across different spatial orientations and examines how side-looking radar observes these differences. The differences observed in signal recovery based on various polarization and orbit are addressed in the second research question, while the first research question primarily examines whether general selective logging-related disturbances have recovered.

Side-looking Radar

This study specifically focuses on two geometric effects: foreshortening and shadow. All selective logging-related disturbance types exhibit faster recovery in Descending orbits compared to Ascending orbits (refer to Figure 9). Regarding logging events, radar shadows persistently appear regardless of whether the sensor detects large or small logging events from either the left or right side, in contrast to vertical or horizontal roads. As a result, areas affected by radar shadowing may exhibit delayed signal recovery compared to areas with more open canopy cover or less obstructed by surrounding vegetation (Lavorel and Garnier, 2002; Wu et al., 2014; Coradini et al., 2022). Additionally, in ascending orbits, where satellites move from south to north, features may be less affected by foreshortening (refer to Figure 10), and shadows may persist for longer durations. This might explain why the signal recovery time for ascending orbits is longer.

In terms of the orbit, this study noted that the signal recovery of VV polarization was quicker than that of VH polarization. The VV polarization is particularly sensitive to double bounce scattering, whereas the VH polarization is more sensitive to volume scattering. This distinction allows for more effective capture of changes in vegetation density and structure (Baghdadi et al., 2017; El Hajj et al., 2017), potentially leading to earlier detection of recovery (Nasirzadehdizaji et al., 2019). Additionally, VV polarization is more sensitive to surface roughness, which leads to higher backscatter returns and may provide clearer signals of changes in vegetation density and recovery (Jacome et al., 2013).

Logging roads are often constructed for short-term use during logging operations. After the logging is completed, these roads are often abandoned and not maintained. Over time, nature begins to reclaim these areas, leading to a slow recovery process. On the other hand, skid roads—typically smaller paths situated at the periphery of a forest or logged area—may experience quicker recovery (Guariguata and Dupuy, 1997). This can be attributed to factors such as their reduced size and lesser environmental disruption compared to larger roads (Watkins et al., 2003).

Related to large-sized and small-size logging events, as seen in Figure 12, the large-sized logging events take longer to recover compared to smaller-scale logging events. This supported by Milodowski et al. (2021), who used LiDAR technology to assess the impacts of selective logging on canopy structure across a gradient of logging intensities and found that the recovery of forest canopy structure from larger-scale logging events is indeed slower. PurdueUniversity (2024) found that forests with more complex canopy structures seemed better able to withstand and recover from the disturbances.

6.3 RQ3: Signal Recovery Characterization

In addressing the third research question, we examined the level of recovery and temporal recovery in selective logging-related activities (as discussed in section 5.3). By integrating spatial patterns recovery map with temporal recovery, we investigated the relationship

between recovery levels and durations. We identified pixels that exhibited high levels of recovery within short time frames, indicating recovery processes. These findings are pertinent to the effect of spatial orientation, particularly highlighting the quicker recovery of the edge of logging roads and logging events within one year.

In relation to recovery metrics, many studies have utilized recovery metrics. This study attempts to apply similar recovery metrics used in optical data to radar data. The objective of incorporating these additional time series metrics is not to determine their reliability or superiority, but rather to gain a comprehensive understanding. Each of the three recovery metrics offers distinct insights into post-disturbance signal recovery.

Optical imagery has been effectively utilized to evaluate forest recovery through three key metrics: RRI, R80p, and YrYr (Pickell et al., 2016; Frazier et al., 2018; White et al., 2022; De Keersmaecker et al., 2022). This study adapts and applies these metrics to radar data, demonstrating their efficacy in capturing temporal dynamics of signal recovery following forest disturbances. The RRI metric quantitatively measures recovery intensity, particularly beneficial in areas with diverse and heterogeneous signals before and after disturbance (Kennedy et al., 2012). Similarly, the R80p metric distinguishes recovery differences between pre-disturbance and forest recovery processes occurring over time (Pickell et al., 2016). Additionally, the YrYr metric facilitates the analysis of temporal recovery patterns over multiple years, capturing annual post-disturbance growth (Frazier et al., 2018)

The successful application of these metrics in radar data underscores the importance of exploring innovative methodologies to leverage the full potential of remote sensing data for environmental monitoring and management.

6.4 SAR for Monitoring Forest Recovery

Upon analyzing signal recovery within three years after disturbance using Sentinel-1 data and our developed method, it becomes evident that while some pixels have shown signs of recovery, not all areas have experienced the same level of regrowth. Specifically, our findings reveal that in Descending VV polarization, the top quartile of data pixels have shown signs of recovery. However, it's important to note that signal recovery does not necessarily equate to actual tree regrowth. Despite observing some pixels that have seemingly recovered to pre-disturbance levels in the Sentinel-1 image within three years, it's important to recognize that actual forest recovery is a much more complex and time-consuming process, often spanning many years. While SAR data, such as that from Sentinel-1, provides valuable insights into vegetation dynamics and can detect changes in the radar backscatter signal, it has limitations when it comes to directly assessing the full extent of vegetation recovery.

One key limitation is that SAR signals primarily reflect changes in vegetation structure and moisture content rather than directly quantifying vegetation biomass, encompassing additional factors such as species composition, density, and carbon content. As a result, the observed signal recovery in radar data may not necessarily correspond to the actual regrowth of forest vegetation. Furthermore, the recovery process of forests

involves various stages, including the re-establishment of vegetation cover, structural development, and ecological succession, which occur over extended timeframes.

Given these limitations, it's crucial to interpret radar data findings cautiously when monitoring recovery. While radar data can provide valuable insights into early-stage recovery dynamics and identify areas showing signs of regrowth, it should be complemented with other data sources, such as field observations, high-resolution optical imagery, and ecological models, to comprehensively understand recovery progress. An integrated approach that combines radar data with other datasets, including L-band radar and optical imagery, and incorporating ecological knowledge and field observations, is essential for effective monitoring and managing forest ecosystems over the long term.

7 Limitations and Recommendations

Several limitations are associated with each of the recommendations provided for assessing signal recovery using radar data, emphasizing the need for future research to address these constraints.

1. The study detected signal recovery by averaging the mean of each window in a temporal moving window approach, relative to the pre-disturbance period. While using five consecutive points within the recovery zone can provide a general view of signal recovery, incorporating additional statistical tests such as ANOVA and T-tests alongside the current method may enhance the robustness of the assessment. These tests could be employed to evaluate various aspects, such as comparing mean recovery values between different experimental conditions or groups (e.g., different regions) using ANOVA and conducting pairwise comparisons of mean recovery values using T-tests. Additionally, ANOVA can assess overall recovery trends and variability among groups, while T-tests can identify significant differences at specific time points or between treatments.

2. While this study focused on utilizing C-band radar data, which is effective for observing volume scatter with secondary and primary branches, it is important to consider incorporating L-band radar. L-band radar data, with its longer wavelength, is more sensitive to changes in biomass, particularly as forest canopies close. However, it's essential to acknowledge that L-band radar may encounter similar challenges as observed for C-band radar in this study, such as issues related to side-looking radar that can lead to radar shadow, which can impact recovery assessments. Therefore, given the advantages of L-band radar in penetrating parts of the canopy and detecting biomass changes, incorporating L-band radar alongside C-band radar could provide complementary information, particularly in environments with dense vegetation cover.

3. While this study did not explore testing various parameters for speckle filtering, noise correction, and terrain flattening, it should be noted that the GRD data used was already multi-looked, potentially minimizing the influence of these parameters, as demonstrated in the detection of disturbances (Balling et al., 2023). Nevertheless, investigating different parameters in future research may be worth to try to evaluate their potential impact on signal recovery.

4. One consideration regarding spatial orientation is disturbance distribution. For future research, employing spatial interpolation techniques like kriging could be valuable for analyzing spatial patterns and heterogeneity associated with selective logging disturbances. This analysis could help understand the influence of different logging event sizes on signal recovery.

5. While this study focuses on signal recovery rather than the actual regrowth of trees within a 2- or 3-year timeframe, it's important to clarify that the signal recovery doesn't necessarily indicate the absence of tree regrowth. Furthermore, integrating L-band data and comparing it with optical data, which is already better understood, could provide valuable insights.

References

Aguilar-Amuchastegui, N., Riveros, J. C., and Forrest, J. L. (2014). Identifying areas of deforestation risk for redd+ using a species modeling tool. *Carbon balance and management*, 9:1–10.

Antropov, O., Rauste, Y., Väänänen, A., Mutanen, T., and Häme, T. (2016). Mapping forest disturbance using long time series of sentinel-1 data: Case studies over boreal and tropical forests. In *2016 IEEE International Geoscience and Remote Sensing Symposium (IGARSS)*, pages 3906–3909. IEEE.

Aquino, C., Mitchard, E. T., McNicol, I. M., Carstairs, H., Burt, A., Puma Vilca, B. L., Obiang Ebanéga, M., Modinga Dikongo, A., Dassi, C., Mayta, S., et al. (2022). Reliably mapping low-intensity forest disturbance using satellite radar data. *Frontiers in Forests and Global Change*, 5.

Baghdadi, N., El Hajj, M., Zribi, M., and Bousbih, S. (2017). Calibration of the water cloud model at c-band for winter crop fields and grasslands. *Remote Sensing*, 9(9):969.

Balling, J., Herold, M., and Reiche, J. (2023). How textural features can improve sar-based tropical forest disturbance mapping. *International Journal of Applied Earth Observation and Geoinformation*, 124:103492.

Bamler, R. (2000). Principles of synthetic aperture radar. *Surveys in Geophysics*, 21(2):147–157.

Bouvet, A., Mermoz, S., Ballère, M., Koleck, T., and Le Toan, T. (2018). Use of the sar shadowing effect for deforestation detection with sentinel-1 time series. *Remote Sensing*, 10(8):1250.

Chirici, G., Giannetti, F., Mazza, E., Francini, S., Travaglini, D., Pegna, R., and White, J. C. (2020). Monitoring clearcutting and subsequent rapid recovery in mediterranean coppice forests with landsat time series. *Annals of Forest Science*, 77(2):1–14.

Coradini, K., Krejčová, J., and Frouz, J. (2022). Potential of vegetation and woodland cover recovery during primary and secondary succession, a global quantitative review. *Land Degradation & Development*, 33(3):512–526.

De Keersmaecker, W., Rodríguez-Sánchez, P., Milencović, M., Herold, M., Reiche, J., and Verbesselt, J. (2022). Evaluating recovery metrics derived from optical time series over tropical forest ecosystems. *Remote Sensing of Environment*, 274:112991.

Decuyper, M., Chávez, R. O., Lohbeck, M., Lastra, J. A., Tsendbazar, N., Hackländer, J., Herold, M., and Vågen, T.-G. (2022). Continuous monitoring of forest change dynamics with satellite time series. *Remote Sensing of Environment*, 269:112829.

Doblas, J., Reis, M. S., Belluzzo, A. P., Quadros, C. B., Moraes, D. R., Almeida, C. A., Maurano, L. E., Carvalho, A. F., Sant'Anna, S. J., and Shimabukuro, Y. E. (2022). Deter-r: An operational near-real time tropical forest disturbance warning system based on sentinel-1 time series analysis. *Remote Sensing*, 14(15):3658.

El Hajj, M., Baghdadi, N., Zribi, M., and Bazzi, H. (2017). Synergic use of sentinel-1 and sentinel-2 images for operational soil moisture mapping at high spatial resolution over agricultural areas. *Remote Sensing*, 9(12):1292.

ESA (2022). Sentinel-1 observation scenario [www document]. , URL "https://sentinels.copernicus.eu/web/sentinel/user-guides/sentinel-1-sar/acquisition-modes".

Filipponi, F. (2019). Sentinel-1 grd preprocessing workflow. In *International Electronic Conference on Remote Sensing*, page 11. MDPI.

Flores, B. M., Holmgren, M., Xu, C., Van Nes, E. H., Jakovac, C. C., Mesquita, R. C., and Scheffer, M. (2017). Floodplains as an achilles' heel of amazonian forest resilience. *Proceedings of the National Academy of Sciences*, 114(17):4442–4446.

Frazier, R. J., Coops, N. C., and Wulder, M. A. (2015). Boreal shield forest disturbance and recovery trends using landsat time series. *Remote Sensing of Environment*, 170:317–327.

Frazier, R. J., Coops, N. C., Wulder, M. A., Hermosilla, T., and White, J. C. (2018). Analyzing spatial and temporal variability in short-term rates of post-fire vegetation return from landsat time series. *Remote Sensing of Environment*, 205:32–45.

Frolking, S., Palace, M. W., Clark, D., Chambers, J. Q., Shugart, H., and Hurtt, G. C. (2009). Forest disturbance and recovery: A general review in the context of spaceborne remote sensing of impacts on aboveground biomass and canopy structure. *Journal of Geophysical Research: Biogeosciences*, 114(G2).

Gaveau, D. (2018). Drivers of forest loss in papua and west papua. *change*, 2001(2018).

GlobalForestWatch (2023). Location of tree cover loss in papua barat, indonesia. Accessed: 2023-09-18 from www.globalforestwatch.org.

Guariguata, M. R. and Dupuy, J. M. (1997). Forest regeneration in abandoned logging roads in lowland costa rica 1. *Biotropica*, 29(1):15–28.

Harfenmeister, K., Spengler, D., and Weltzien, C. (2019). Analyzing temporal and spatial characteristics of crop parameters using sentinel-1 backscatter data. *Remote Sensing*, 11(13):1569.

Hird, J. N., Kariyeva, J., and McDermid, G. J. (2021). Satellite time series and google earth engine democratize the process of forest-recovery monitoring over large areas. *Remote Sensing*, 13(23):4745.

Jacome, A., Bernier, M., Chokmani, K., Gauthier, Y., Poulin, J., and De Sève, D. (2013). Monitoring volumetric surface soil moisture content at the la grande basin boreal wetland by radar multi polarization data. *Remote Sensing*, 5(10):4919–4941.

Jones, H. P. and Schmitz, O. J. (2009). Rapid recovery of damaged ecosystems. *PloS one*, 4(5):e5653.

Kennedy, R. E., Yang, Z., Cohen, W. B., Pfaff, E., Braaten, J., and Nelson, P. (2012). Spatial and temporal patterns of forest disturbance and regrowth within the area of the northwest forest plan. *Remote Sensing of Environment*, 122:117–133.

Kurbanov, E., Vorobev, O., Lezhnin, S., Sha, J., Wang, J., Li, X., Cole, J., Dergunov, D., and Wang, Y. (2022). Remote sensing of forest burnt area, burn severity, and post-fire recovery: a review. *Remote Sensing*, 14(19):4714.

Lavorel, S. and Garnier, E. (2002). Predicting changes in community composition and ecosystem functioning from plant traits: revisiting the holy grail. *Functional ecology*, 16(5):545–556.

Meng, R., Wu, J., Zhao, F., Cook, B. D., Hanavan, R. P., and Serbin, S. P. (2018). Measuring short-term post-fire forest recovery across a burn severity gradient in a mixed pine-oak forest using multi-sensor remote sensing techniques. *Remote Sensing of Environment*, 210:282–296.

Milodowski, D. T., Coomes, D. A., Swinfield, T., Jucker, T., Riutta, T., Malhi, Y., Svátek, M., Kvasnica, J., Burslem, D. F., Ewers, R. M., et al. (2021). The impact of logging on vertical canopy structure across a gradient of tropical forest degradation intensity in borneo. *Journal of Applied Ecology*, 58(8):1764–1775.

Morresi, D., Vitali, A., Urbinati, C., and Garbarino, M. (2019). Forest spectral recovery and regeneration dynamics in stand-replacing wildfires of central apennines derived from landsat time series. *Remote Sensing*, 11(3):308.

Mullissa, A., Vollrath, A., Odongo-Braun, C., Slagter, B., Balling, J., Gou, Y., Gorelick, N., and Reiche, J. (2021). Sentinel-1 sar backscatter analysis ready data preparation in google earth engine. *Remote Sensing*, 13(10):1954.

Nasirzadehdizaji, R., Balik Sanli, F., Abdikan, S., Cakir, Z., Sekertekin, A., and Ustuner, M. (2019). Sensitivity analysis of multi-temporal sentinel-1 sar parameters to crop height and canopy coverage. *Applied Sciences*, 9(4):655.

Park, S.-E., Ferro-Famil, L., Allain, S., and Pottier, E. (2014). Surface roughness and microwave surface scattering of high-resolution imaging radar. *IEEE Geoscience and Remote Sensing Letters*, 12(4):756–760.

Pickell, P. D., Hermosilla, T., Frazier, R. J., Coops, N. C., and Wulder, M. A. (2016). Forest recovery trends derived from landsat time series for north american boreal forests. *International Journal of Remote Sensing*, 37(1):138–149.

PlanetTeam (2017). Planet application program interface: In space for life on earth. San Francisco, CA.

PurdueUniversity (2024). Title of the article. *Science Daily*. Retrieved from https://www.sciencedaily.com/releases/2024/02/240206151501.htm.

Raharjo, S., Suarga, E., Rosyaridho, M. F., Kalmirah, J., et al. (2022). Towards low carbon development strategies from forestry sector in west papua. In *IOP Conference Series: Earth and Environmental Science*, volume 989, page 012007. IOP Publishing.

Reiche, J., Mullissa, A., Slagter, B., Gou, Y., Tsendbazar, N.-E., Odongo-Braun, C., Vollrath, A., Weisse, M. J., Stolle, F., Pickens, A., et al. (2021). Forest disturbance alerts for the congo basin using sentinel-1. *Environmental Research Letters*, 16(2):024005.

Romijn, E., Ainembabazi, J. H., Wijaya, A., Herold, M., Angelsen, A., Verchot, L., and Murdiyarso, D. (2013). Exploring different forest definitions and their impact on developing redd+ reference emission levels: A case study for indonesia. *Environmental Science & Policy*, 33:246–259.

Schaufler, S., Bauer-Marschallinger, B., Hochstöger, S., and Wagner, W. (2018). Modelling and correcting azimuthal anisotropy in sentinel-1 backscatter data. *Remote sensing letters*, 9(8):799–808.

Sidle, R. C., Sasaki, S., Otsuki, M., Noguchi, S., and Rahim Nik, A. (2004). Sediment pathways in a tropical forest: effects of logging roads and skid trails. *Hydrological processes*, 18(4):703–720.

Surovỳ, P. and Kuželka, K. (2019). Acquisition of forest attributes for decision support at the forest enterprise level using remote-sensing techniques—a review. *Forests*, 10(3):273.

Tanase, M., de la Riva, J., Santoro, M., Pérez-Cabello, F., and Kasischke, E. (2011). Sensitivity of sar data to post-fire forest regrowth in mediterranean and boreal forests. *Remote Sensing of Environment*, 115(8):2075–2085.

Turubanova, S., Potapov, P. V., Tyukavina, A., and Hansen, M. C. (2018). Ongoing primary forest loss in brazil, democratic republic of the congo, and indonesia. *Environmental Research Letters*, 13(7):074028.

Watkins, R. Z., Chen, J., Pickens, J., and Brosofske, K. D. (2003). Effects of forest roads on understory plants in a managed hardwood landscape. *Conservation Biology*, 17(2):411–419.

White, J. C., Hermosilla, T., Wulder, M. A., and Coops, N. C. (2022). Mapping, validating, and interpreting spatio-temporal trends in post-disturbance forest recovery. *Remote Sensing of Environment*, 271:112904.

Wu, G.-L., Zhao, L.-P., Wang, D., and Shi, Z.-H. (2014). Effects of time-since-fire on vegetation composition and structures in semi-arid perennial grassland on the loess plateau, china. *Clean–Soil, Air, Water*, 42(1):98–103.

Yudha, R. P., Sugito, Y. S., Sillanpää, M., and Nurvianto, S. (2021). Impact of logging on the biodiversity and composition of flora and fauna in the mangrove forests of bintuni bay, west papua, indonesia. *Forest Ecology and Management*, 488:119038.

Zhao, F. R., Meng, R., Huang, C., Zhao, M., Zhao, F. A., Gong, P., Yu, L., and Zhu, Z. (2016). Long-term post-disturbance forest recovery in the greater yellowstone ecosystem analyzed using landsat time series stack. *Remote Sensing*, 8(11):898.